Check for updates

Ultra-sharp and surfactant-free silver nanowire for scanning tunneling microscopy and tip-enhanced Raman spectroscopy†

Qiushi Liu, ‡[a] Sanggon Kim, ‡[b] Xuezhi Ma, [a] Ning Yu, [b] Yangzhi Zhu, [b] Siyu Deng,[a] Ruoxue Yan, *[b,c] Huijuan Zhao [d] and Ming Liu*[a,c]

Chemically-synthesized single-crystalline silver nanowire (AgNW) probes can combine the scanning tunneling microscopy (STM) technique with tip-enhanced Raman scattering spectroscopy (TERS) for complementary morphological and chemical information with nanoscale spatial resolution. However, its performance has been limited by the blunt nanowire tip geometry, the insulating surfactant layer coating AgNW surfaces, and the thermal-induced mechanical vibrations. Here, we report a reproducible fabrication method for the preparation of sharp-tip AgNW-based TERS probes. By removing the polyvinylpyrrolidone (PVP) surfactant molecules from the AgNW surfaces for stable electrical conductivity and controlling the protruding length with μm-level accuracy for improved mechanical stability, we demonstrate atomic-resolution STM imaging with the sharp-tip AgNW probe. Furthermore, the sharp-tip AgNW has an excellent TER enhancement (~1.1×10^6), which is about 66 folds of that achieved by regular AgNWs. Our experiments demonstrate that AgNWs with clean interfaces and the proper tip geometry can provide reliable and reproducible STM and TER characterizations, which remove the hurdles preventing the implementation of AgNW in STM-based near-field optical applications for a broad community.

Introduction

The techniques to acquire both topographical and chemical information with nanoscale spatial resolution have intrigued broad research interest, due to the increasing demands of such capability in nanotechnology and material science. Although topographical information can be readily acquired with high spatial resolution *via* conventional characterization tools including electron microscopy and scanning probe microscopy (SPM), mapping the chemical information at a similar scale remains challenging. Raman scattering vibrational spectroscopy is a powerful nondestructive technique for the investigation of the chemical bonding, composition, physical states and photon confinement of various types of materials. Integrating Raman spectroscopy with SPM techniques[1] has been demonstrated to break the optical diffraction limit that restricts the spatial resolutions of the conventional Raman imaging. This integration leads to the development of the tip-enhanced Raman spectroscopy (TERS)[2] imaging technique, which combines the high spatial resolution of SPM with the surface-plasmon-enhanced Raman signal through the use of a sharp metal tip.[3–5] As a result, the quality and reproducibility of TERS images profoundly rely on the morphology and the plasmonic enhancement factor of the metallic probes. The probe-preparation techniques have been at the heart of TERS imaging.[5–11]

Ever since its first experimental demonstration in 2000,[1,5,12] a number of probe preparation methods have been developed for TERS measurements, including metal deposition on conventional AFM probes[6,7] and the electrochemical etching of metal needles.[8] Various illumination methods, such as bottom-illumination,[13] side-illumination,[14] and top-illumination[15] methods, have been examined and enhancement factors (EF) between 10^2–10^4 have been reported on numerous samples including organic dyes,[16] low-dimensional materials,[17] and biological molecules.[18] However, it remains challenging to prepare high-performance probes with reasonable reliability and consistency with these methods,[9–11] which have become a major obstacle against TERS applications.

[a]*Department of Electrical and Computer Engineering, Bourns College of Engineering, University of California-Riverside, Riverside, California 92521, USA. E-mail: mingliu@ucr.edu*

[b]*Department of Chemical and Environmental Engineering, Bourns College of Engineering, University of California-Riverside, Riverside, California 92521, USA. E-mail: rxyan@engr.ucr.edu*

[c]*Material Science Engineering program, Bourns College of Engineering, University of California-Riverside, Riverside, California 92521, USA*

[d]*Department of Mechanical Engineering, Clemson University, Clemson, SC 29634-0921, USA*

†Electronic supplementary information (ESI) available. See DOI: 10.1039/c8nr08983c

‡These authors contribute equally.

Recently, the AgNW synthesized by polyol process[19] has been considered as a promising candidate for reliable TERS probe preparation,[20,21] due to its high synthesis yield, outstanding plasmonic performance,[20–23] and excellent mechanical properties[24] for SPM applications. By assembling AgNWs with conventional cantilever probes, high-aspect-ratio AFM probes have been demonstrated.[25] The plasmonic hotspot supported by the AgNW tip is also expected to be suitable for TERS measurements with high spatial resolution and sensitivity, in particular when STM is employed. However, the practical implementation of AgNWs for STM imaging is facing three major obstacles. Firstly, polyvinylpyrrolidone (PVP) molecules, an essential surfactant used for the one-dimensional growth of AgNWs,[26] form an electrical insulating layer on the AgNW surface and hinder the charge transfer processes, including the charge transfer from the STM electrode to the AgNW probe and from the AgNW probe to the sample substrate. Secondly, most AgNWs synthesized by the polyol synthesis have round or even flat tip shapes[27] due to the oxidative etching during the sample synthesis and storage, which decrease both the STM and the TERS resolutions. Lastly, the common method to prepare AgNW probes utilizes the alternating current-dielectrophoresis (ac-DEP) force to attach AgNWs onto metallic tips,[10,11,21] which tend have long protruding AgNW regions since the attaching locations are random. The long protruding length leads to large vibrational noises and cannot provide atomic resolution imaging. Moreover, the ac-DEP method requires the surfactant coating layer on AgNWs to maintain their dispersion in solution, resulting in poor electrical conductivity in the prepared probes that are not suitable for STM imaging. In this work, we investigate the influences of the surfactant layer, the AgNW tip shape, and the protruding length on STM imaging quality (Fig. 1). We also report a reliable TERS probe fabrication method which utilizes a micromanipulator to mount a sharp-tip surfactant-free silver nanowire (AgNW) onto a tungsten probe with μm accuracy. By comparing the performance of sharp-tip AgNWs with regular ones, we prove that the Raman enhancement factor can be improved by 60 folds on a monolayer graphene sample.
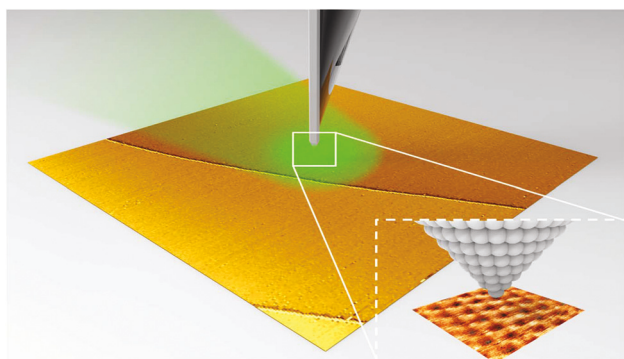
Fig. 1 Schematic illustration of using a sharp-tip silver nanowire probe for STM-TERS. Inset: An atomic-resolution image of HOPG surface acquired by the probe.

Results and discussion

Firstly, we examined the PVP layer thickness on AgNW cleaned with a conventional purification method using ethanol and centrifugation.[11,28] The TEM images show a significant reduction of PVP layer thickness after washing with ethanol for 6 times, as compared with the pristine AgNWs (Fig. 2a and c–i). Additional washing cannot remove the PVP layer below 1 nm,[28] even with rigorous vortex or sonication. On the other hand, oxidation of Ag arises due to the diffusion of the oxygen into the washing solution during the prolonged purification period. The PVP residues can significantly reduce the STM performance of a AgNW probe, by requiring high bias voltage (>1 V) to initiate the tunneling current, reducing the current-distance sensitivity and introducing the PVP molecule contamination during the scanning. Furthermore, as shown in the tunneling current characteristic at different probe-to-sample gap distance (Fig. 2d, red curve), there is no significant current change with the decrease of the gap distance when a PVP-coated AgNW is used, due to the blockage of the thin PVP layer (~1 nm). Tip cleaning process using high voltage pulses (5 V) may partially remove the PVP molecules from the AgNW apex, but no measurable improvement on the scanning results was observed. This may originate from the difficulty in removing the long-chain PVP molecules (~55k in molecule weight) attached at the proximity of the tip apex, which can be dragged into the gap by the sample substrate during the scanning process and influence the tunneling current. The low current-distance sensitivity results in poor STM imaging quality on a gold substrate (Fig. 2c (iii)). To fully remove the PVP residues left by the regular purification method, we used the sodium borohydride ($NaBH_4$) solution that has been demonstrated as an efficient adsorbate stripper for various chemicals, including organothiols, rhodamine, and PVP, from metal surfaces via the hydride of the absorbate.[29,30] To avoid the fast oxidation of fresh silver surfaces, which is within hours in water without the protection of a PVP layer, we conducted the purification process in deoxygenated $NaBH_4$ solution purged and stirred by bubbles from high-flow-rate nitrogen gas, as shown in Fig. 2b. This PVP removal method prevents oxidation of the AgNW after the complete desorption of the PVP layer from the nanowire surface and the vigorous stirring with the nitrogen bubbles accelerates the desorption of the PVP layer. Complete removal of the PVP layer from the surface of AgNW was confirmed with TEM images (Fig. 2c (ii)) and the significant improvement in current-distance measurement was achieved (Fig. 2d, blue curve). After the thorough purification, the AgNW probe has the similar current-distance characteristic as a freshly prepared platinum/iridium (Pt/Ir) probe (Fig. 2d, green curve), indicating that the PVP residues are reduced to a negligible level. It is worth noting that the work functions obtained for both Ag and Pt/Ir are significantly smaller than other experimental values, which may due to the surface contamination of the sample substrate under the ambient condition.[31] The STM scanning result of an Au film using the PVP-removed AgNW probe clearly shows the grains of deposited gold, as shown in Fig. 2c(iv).
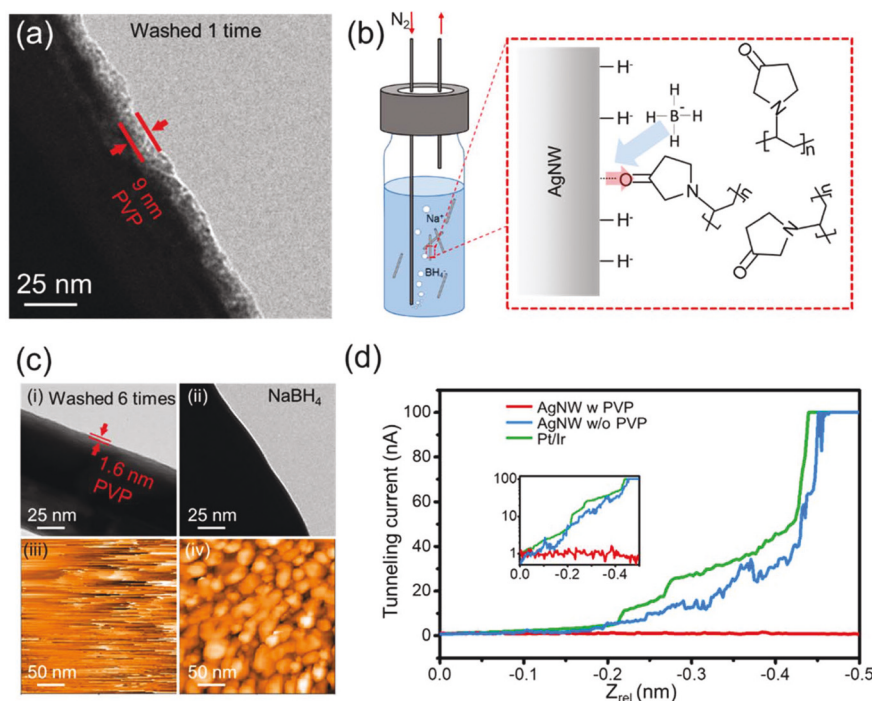
Fig. 2 Removal of surfactant molecules from AgNW surfaces and its impacts on STM imaging. (a) TEM confirms that the as-prepared AgNWs are coated by a thin layer (~9 nm) of PVP molecules, which serve as the surface surfactant during the salt-mediated polyol process. (b) Schematic illustration of the surfactant removal process. Nitrogen bubbles are generated to stir the $NaBH_4$ solution while maintaining the N_2 environment to avoid the oxidation of AgNWs. Inset: The detachment of PVP from Ag surface by hydride generated from the boron hydride. (c) Comparison of AgNWs prepared by the conventional cleaning method (6 times of washing with ethanol, inset i) and the NaBH4 cleaning method (inset ii). The conventional method leaves ~1.6 nm of PVP residues that result in a poor STM image quality as shown in (iii). AgNWs treated by $NaBH_4$ cleaning have PVP-free surface and can serve as STM probes for topographical imaging (iv) (STM conditions: −1 V probe bias, −1 nA tunneling current). (d) Comparison of tunneling current variations as a function of the probe movement toward the substrate (probe bias: −1 V).

The shape of a AgNW tip can significantly influence the STM quality. AgNWs synthesized with conventional polyol process through the salt-mediated agents have rounded or even flap tip shape as shown in Fig. 3b–i, originating from etching in the existence of oxygen and Cl⁻ during the synthesis.[32] Multi-channel effect occurs when blunt-tip AgNWs are used, resulting in low spatial resolutions and ghosting images. Fig. 3c shows the STM scanning image of single-walled carbon nanotubes (SWCNTs) dispersed on a Au film, using a AgNW probe with round tip geometry. The cross-sectional analysis reveals that a 1.4 nm-in-height SWCNT bundle has a width of 34 nm, which is overestimated due to the blunt AgNW tip shape. In order to reduce the tip radius, a modified copper chloride-mediated polyol method has been exploited for sharp-tip AgNWs.[25] By increasing the growth rate to faster than the PVP passivation rate (Fig. 3a), AgNWs with conical tips could be synthesized. The sharp-tip AgNW with a small tip radius ~5 nm can provide a much finer STM resolution on the same SWCNT sample (Fig. 3d). In particular, the sharp tip allows to image trenches such as the gaps between CNT bundles (inset of Fig. 3d). It also enables a drastic enhancement of the TERS performance which is discussed in a following section.

Besides the PVP insulating layer and the AgNW tip radius, another determining factor for high-quality STM imaging is

the vibration of the nanowire, which can be attributed to acoustic pressure-induced vibration and thermally induced vibration. The acoustic noise level in a quiet room is around 20–40 dB and reaches ~60 dB in a research laboratory, generating a root-mean-squared (r.m.s.) displacement on the free-standing AgNW that can be estimated by the Euler–Bernoulli beam theory,[33]

$$\langle \mathrm{r.m.s._{acoustic}} \rangle = \frac{qL^4}{\sqrt{2} \times 8EI} \tag{1}$$

where q is a uniform distributed load per unit length, L is the length of the nanowire, E is the modulus of elasticity, which is reported ~90 GPa for AgNW,[34] and I is the area moment of inertia for a cylindrical cantilever. q can be estimated by $q = P \cdot a$, where P is the acoustic pressure and a is the nanowire diameter. The acoustic noise level (L_P) measured in dB is defined by

$$L_P = 20 \log_{10} \frac{P}{P_0} (\mathrm{dB}) \tag{2}$$

where P_0 is reference acoustic pressure (20 µPa). For a typical AgNW with the diameter between 100–300 nm, the free-standing protruding region must be shorter than ~20 µm in order
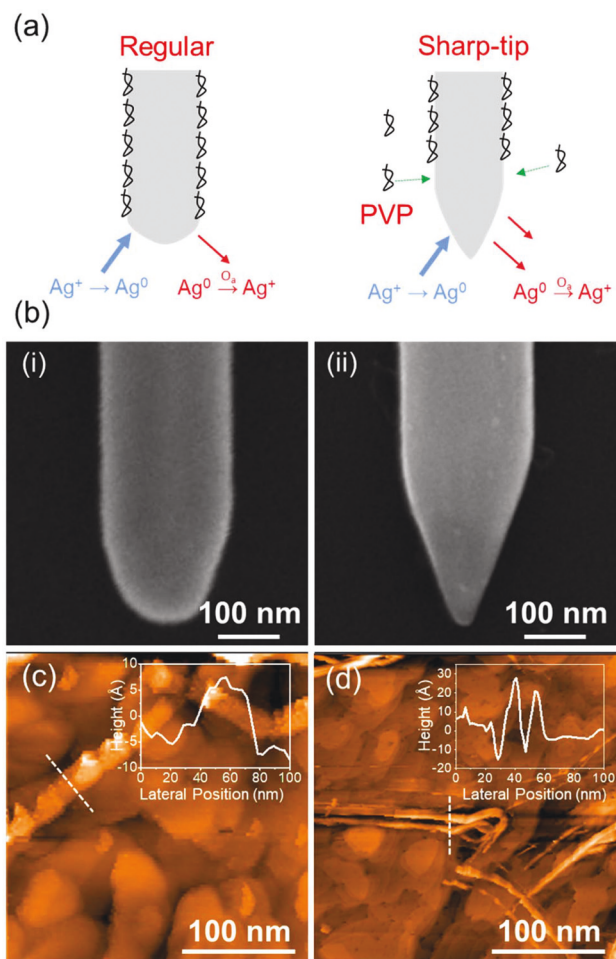
Fig. 3 Influence of AgNW tip radius on STM scanning. (a) Schematic illustration of AgNW sharpening process by controlling the AgNW growth, oxidative etching, and PVP passivation rates occurring at the tip of AgNW. (b) SEM images of AgNW produced by the regular polyol synthesis method and the sharp-tip nanowire synthesis method. The AgNW probes in (i) and (ii) are used to get scanning results on a SWCNT sample, shown in (c) and (d), respectively. Insets: The cross-sectional profiles along the dashed lines. STM conditions: probe bias −200 mV, tunneling current −0.4 nA.

to have the acoustic vibration amplitude less than 1 Å under 60 dB environmental noise.

The thermal fluctuation of a AgNW can be estimated according to the equipartition theorem. Every independent quadratic term of a cantilever oscillator system in the thermal equilibrium has a mean value of $\frac{1}{2}k_{\mathrm{B}}T$, where k_{B} is the Boltzmann constant and T is the absolute temperature. A cantilever with a spring constant K and mean square deflection $\langle x^2 \rangle$ has a potential energy of $\frac{1}{2}K\langle x^2 \rangle$ where K is given by $K = \dfrac{3EI}{L^3}$. The equipartition theorem gives $\frac{1}{2}k_{\mathrm{B}}T = \frac{1}{2}K\langle x^2 \rangle$ which can be used to estimate the amplitude of the thermally induced root-mean-square oscillation of a cantilever with a free end:

$$\langle \mathrm{r.m.s._{thermal}} \rangle_{25^{\circ}\mathrm{C}} = 5.6 \times 10^{-3} \frac{L^{3/2}}{a^2} \text{ Å}. \tag{3}$$

This equation is valid at 25 °C, with a and L in the unit of μm. To achieve the atomic-resolution STM imaging, the protruding length of a 200 nm-in-diameter AgNW needs to be shorter than 3.7 μm to reduce the thermal noise level to less than 1 Å (Fig. 4b). For a narrower AgNW with 100 nm in diameter, this protruding limit is decreased to 1.5 μm. Compared with the acoustic-pressure-induced vibration, the thermally induced vibration dominates in the AgNW-STM system.

Precisely controlling the protruding length of a AgNW on a tungsten tip is consequently essential in suppressing the mechanical noise level for atomic-resolution STM imaging. Previous attempts using the ac-DEP force to attach AgNWs tend to have arbitrary protruding lengths between 10–100 μm, since the adhesion locations induced by ac-DEP force are random. Here, we mount the AgNW onto a tungsten tip using a bench-top micromanipulator to realize the μm-accuracy control of protruding length. The length of the freestanding protruding portion of the AgNW can be adjusted by moving the AgNW along the tungsten tip, and is shortened to less than 2 μm for the low-vibration-noise atomic-resolution STM imaging. Fig. 4a shows the SEM image of a AgNW-STM probe, using a 200 nm-in-diameter AgNW and 2.3 μm in protruding length, yielding around 0.5 Å thermal noise according to eqn (3). To prevent the oxidation of the AgNW and reduce the acoustic noise, the STM scanning head is sealed in a helium chamber during the scanning. The corresponding STM images of a highly-oriented pyrolytic graphite (HOPG) sample taken under ambient conditions are shown in Fig. 4c and d. Clear steps are observed within a 500 nm × 500 nm range scanning, with the cross section (Fig. 4c inset) showing approximately 3.7 Å step height that is close to the single atom layer thickness of graphite. The zoom-in scanning on a flat region of the HOPG in Fig. 4d illustrates the hexagonal structure of carbon atoms, which proves the capability of the prepared AgNW-STM probe for steady raster scanning with atomic resolution.

To gain insight on the TERS performance, we performed full-wave electromagnetic simulations using the finite element analysis (COMSOL Multiphysics 5.1) to assess the field enhancement factor, which is defined as the ratio between the electric field at the tip apex and that of the incident light ($\mathrm{EF_{field}} = E_{\mathrm{tip}}/E_{\mathrm{inc.}}$), over a wavelength range from 400 to 800 nm. As illustrated in Fig. 5a, the 3D simulation geometry contains a silver conical probe vertically placed above a silver substrate with 1 nm gap in between and is illuminated by a diffraction-limited laser beam with p-polarization from the side at 20° incident angle. Fig. 5b depicts the results of a conical tip (tip radius ∼15 nm) excited by a 532 nm laser, which contains a strongly-enhanced highly-localized hotspot at the gap. The cross-section profile of $|E|^2$ reveals that the hotspot has a full width at half maximum (FWHM) of 3.8 nm, much smaller than the tip radius. We calculated both the enhancement factor EF (red curve) and the hotspot size (blue curve) as a function of the tip radius, as shown in Fig. 5c. As the tip radius decreases, the EF increases exponentially, while the size of the electric field FWHM decreases linearly.
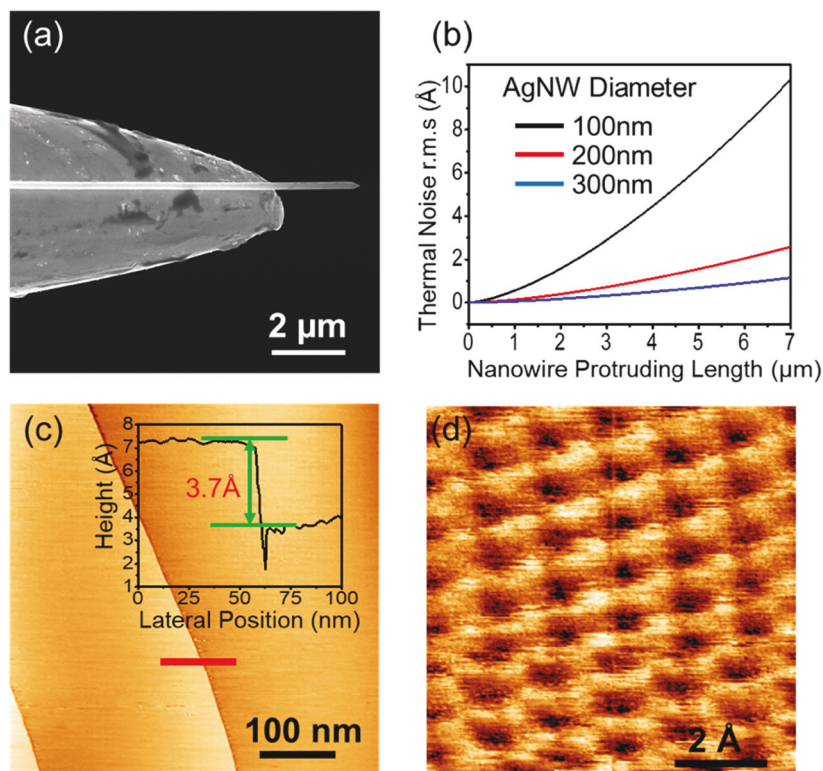
Fig. 4 Atomic-resolution STM images obtained by the sharp-tip AgNW. (a) SEM image of the AgNW probe mounted on a tungsten tip. The protruding length of AgNW is 2.3 μm. (b) Thermally induced vibration under different nanowire diameters (100, 200, and 300 nm). (c) The STM image of HOPH shows a clear and accurate vertical resolution of mono atomic layer. Inset: The cross-sectional profile of the red solid line. (d) Atomic-resolution STM image of HOPG (Probe bias −50 mV, tunneling current −1 nA).
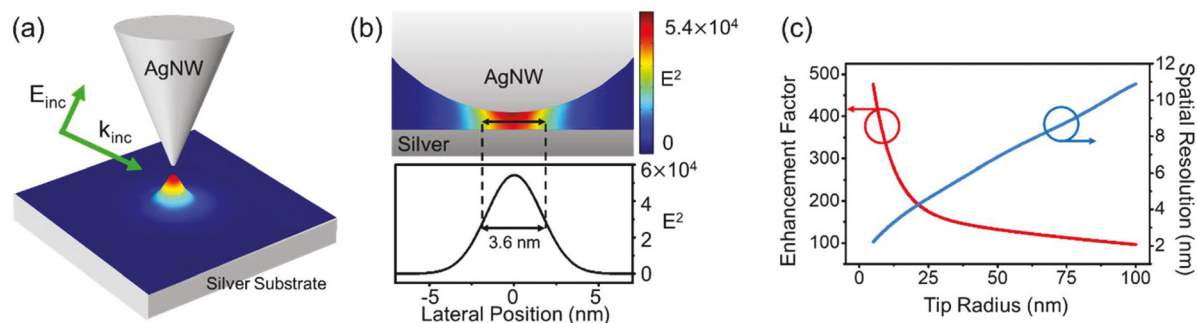
Fig. 5 Electromagnetic simulation of the localized surface plasmon resonance inside the gap formed by a AgNW tip and a metal substrate. (a) Simulation geometry schematic. Simulation conditions: tip radius ~15 nm, gap distance 1 nm, excitation wavelength 532 nm. (b) Zoom-in plot of the intensity ($|E|^2$) distribution at the gap region. Bottom: Intensity profile at the gap reveals a hotspot size of 3.6 nm. (c) Calculated results of field enhancement factor and hotspot size as functions of tip radius.

The Raman spectroscopy measurements were carried out in backscattering geometry using a commercial Raman spectrometer (Horiba Labram HR800), which is equipped with a motorized objective lens holder, a 600 grooves per mm grating, and a long-working-distance 100× with a numerical aperture (NA) of 0.6. The objective mounted on the motorized holder was dedicated to align the incident light (Laser Quantum Ventus, 532 nm, 100 μW at the sample) with the AgNW tip apex and collect the Raman scatterings, as depicted in Fig. 6a. As a proof of functionality, the TERS experiments were performed on a monolayer graphene sample, which was prepared on a copper film by the chemical vapor deposition (CVD) method and transferred on a silver substrate (50 nm in film thickness, deposited on a silicon dioxide wafer) using the PDMS-assisted transfer technique.[35] The surface roughness of the silver film is below 1 nm, which is low enough to suppress the surface-enhanced Raman scattering (SERS) process on the film. The AgNW was mounted onto an AFM cantilever and
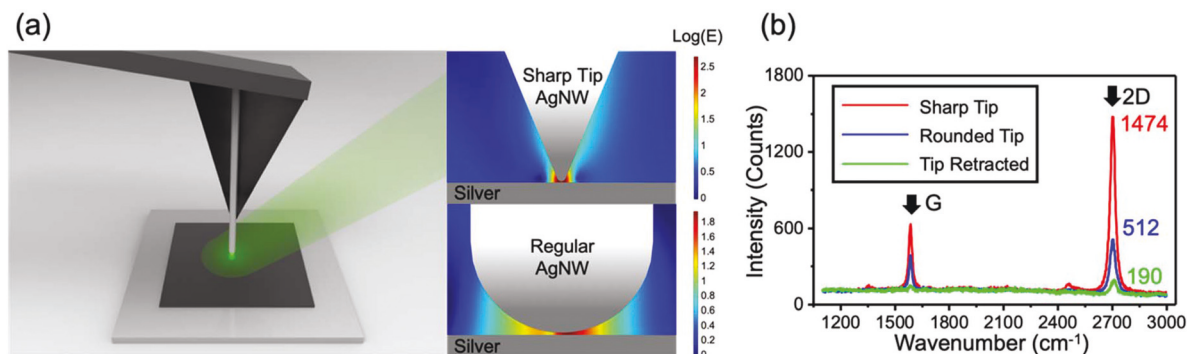
Fig. 6 Tip-enhanced Raman spectroscopy measurement. (a) The schematic of the sharp-tip AgNW for TERS measurement. The AgNW is mounted on an AFM cantilever. A monolayer graphene on a Ag substrate is used to evaluate the Raman enhancement factor. Inset images show the electric field distribution around a sharp-tip AgNW and regular rounded tip. (b) Raman spectra acquired by different AgNW tips. Laser specification: 532 nm in wavelength, 2 mW at the sample surface. Acquisition time 3 s.

launched on the sample surface by an AFM controller for TER spectrum measurement. In order to gain insights into the influence of the AgNW tip shape to the TERS experiment, five sharp-tip and five round-tip AgNWs have been tested on a monolayer graphene sample, with 5 random locations chosen for each probe. Fig. 6 exhibits the averaged TER spectra measured by regular AgNW probes and sharp-tip AgNW probes, in comparison with the Raman spectrum background without the probe launched (green curve). The contrasts for regular probes and sharp-tip probes are 2.7 and 7.7, respectively. All TER spectra show intense spectral features that can be assigned to typical graphene phonon modes, in particular, the G-band at around 1580 cm^{-1} and the 2D peak at around 2680 cm^{-1}. The positions of the G and 2D peaks, the single Lorentzian shape of the 2D peak, the intensity ratio of the 2D to G peaks (~2), and the absence of the D peak (~1350 cm^{-1}) all indicate the high quality of the single layer graphene sample after the transfer process, which is suitable for the evaluation of the TER enhancement.

To estimate the field enhancement achieved with the AgNW probes, we calculate the Raman enhancement factor through the following equation.[36]

$$\text{EF}_{\text{Raman}} = \frac{I_{\text{NF}}}{I_{\text{FF}}} \frac{A_{\text{FF}}}{A_{\text{NF}}} \qquad (4)$$

which considers the normalized Raman intensity by dividing the intensity from the far-field (I_{FF}) and the near-field (I_{NF}) with the corresponding area (A_{FF} and A_{NF}), leading to the enhancement factor that is independent of Raman excitation area. I_{FF} and I_{NF} can be obtained from the spectra in Fig. 6b. The area of excitation A_{NF} is estimated based on the numerical simulation in Fig. 5, yielding around $A_{\text{NF}} = \pi \times (2.5 \text{ nm})^2$ for the sharp-tip AgNW and $A_{\text{NF}} = \pi \times (12 \text{ nm})^2$ for a regular AgNW probe. In contrast, the semi-minor radius of the elliptical laser spot focused by the tilted objective lens (tilt angle ~20°) from the side is diffraction-limited to about $r_{\text{ex,minor}} \approx 0.61 \times \lambda/\text{NA} \approx$ 540 nm, and the semi-major radius is $r_{\text{ex,major}} \approx r_{\text{ex,minor}}/\sin 20° \approx 1580$ nm. The illuminated area is therefore at least

$A_{\text{FF}} = \pi \times (540 \text{ nm}) \times (1580 \text{ nm})$. The Raman enhancement factor can be estimated from eqn (4), which gives 1.1×10^6 for the sharp-tip AgNW probe (Raman intensity contrast = 7.7), a 66-fold increment when compared with the regular AgNW ($\sim 1.6 \times 10^4$, Raman intensity contrast = 2.7). Since the Raman intensity scales approximately with the electric field as $|E|^4$, the EF$_{\text{Raman}}$ corresponds to electric field enhancement (EF$_{\text{field}}$) around 32 for the sharp-tip AgNW and ~11 for the regular AgNW. These values are similar to other sharp TERS tips prepared by pulling and electrochemical etching of gold wires[7] but requires much simpler fabrication.

To conclude, we demonstrate a reliable process for the reproducible fabrication of ultra-clean nanowire-based STM probes. The probes consist of a sharp-tip silver nanowire positioned on a regular metallic probe and can provide atomic-resolution STM imaging on a graphite lattice and topographical mapping of single-walled carbon nanotubes deposited on metal substrates. We confirm that the surfactant residues left on the AgNW surface after conventional cleaning treatment, the tip radius, and the thermal vibration from the protruding part of the AgNW are the major limiting factors for imaging resolution. The promising results imply that the micromanipulation method to assemble sharp-tip AgNWs on metallic tips for STM-TERS applications can be a reliable fabrication technique for a much simplified near-field Raman imaging research.

Methods

AgNW synthesis

AgNWs with round tips were synthesized *via* a modified salt-mediated polyol process. CuCl$_2$ was used as the salt-mediated agent to remove the adsorbed atomic oxygen efficiently from AgNW for less oxidative etching and fast growth.[26] 5 ml ethylene glycol was added in a pear-shaped flask with a stir bar and the flask was immersed in a silicone oil bath at 152 °C under magnetic stirring (400 rpm) for 15 minutes. While heating up

the flask, 6 ml of 0.094 M AgNO$_3$ (99+%, Fisher) and 6 ml of 0.147 M PVP (avg M_w # 55 000, Sigma-Aldrich) in ethylene glycol (EG, 99%, Fisher) were prepared. 80 μl of 4 mM CuCl$_2$ (99.995%, Sigma-Aldrich) was added in the flask and the flask was heated for an additional 15 minutes. Injection of 3 ml of the PVP was conducted into the flask followed by the injection of AgNO$_3$ solution at the injection rate of 125 μl min^{-1} using two syringe pumps.[27] The injection continued for 40 min and the flask was removed from the silicon oil bath and cooled at room temperature for 15 minutes. The synthesized AgNWs were purified with ethanol and centrifugation at 2000 RPM for 20 minutes 5 times. For the ultra-sharp AgNW, we followed the synthesis method described in ref. 25.

Removal of PVP layer from AgNW surface

AgNW in 3 ml of 4 mM NaBH$_4$ was added in a 4 ml glass vial with a septa cap and it was purged with nitrogen supplied with a syringe needle. After 1-hour purification, the solution was refreshed with NaBH$_4$ solution and additional 1-hour purgation was conducted. When the removal process completed, aggregated AgNW could be observed in the solution. The AgNW aggregates were transferred to another clean 4 ml vial with ethanol. A gentle sonication was performed to disperse the AgNWs before using.

Au film and SWCNTs/Au

Au (100 nm in thickness) was deposited on silicon substrates and freshly exfoliated mica layers using e-beam thermal evaporator at the deposition rate of 1 Å s^{-1}. The Au film on a silicon substrate was directly used for the scanning of Au grains. For SWCNTs/Au samples, the ultrasmooth Au film was required, which was prepared by annealing Au/mica at 350 °C for 1 hour. The Au film was then mechanically peeled off by gluing the Au film onto to a silicon substrate. We sprayed SWCNTs (conductive aqueous ink, Sigma-Aldrich) on the Au film at 60 °C. Surfactants used for the dispersion of the SWCNTs in water was removed by immersing the SWCNTs/Au in DI water which is refreshed by the continuous flow of DI water. The SWCNTs/Au sample was dried by blowing gently with a nitrogen gun.

STM scanning

All the scanning images were acquired using a NaioSTM (NanoSurf) apparatus in a hellium chamber.

Full-wave electromagnetic simulation

The 3D simulation geometry (Fig. 5a) contains a conical silver probe (45° tip angle and 15 nm tip apex radius) placed vertically above a silver substrate with 1 nm gap between the tip apex and the substrate. The incident beam with Gaussian-shape profile (532 nm in wavelength, 500 nm in Gaussian width, the maximum electrical field intensity is 1 V m^{-1}) illuminates at the AgNW tip apex from the side with an incident angle of 20°. The permittivity of silver ($-11.76 + 0.37i$) is adopted from Johnson and Christy.[37]

Conflicts of interest

There are no conflicts to declare.

Acknowledgements

References

1 N. Hayazawa, Y. Inouye, Z. Sekkat and S. Kawata, *Opt. Commun.*, 2000, **183**, 333–336.
2 B. Pettinger, B. Ren, G. Picardi, R. Schuster and G. Ertl, *Phys. Rev. Lett.*, 2004, **92**, 096101.
3 L. Novotny and S. J. Stranick, *Annu. Rev. Phys. Chem.*, 2006, **57**, 303–331.
4 L. G. Cancado, A. Hartschuh and L. Novotny, *J. Raman Spectrosc.*, 2009, **40**, 1420–1426.
5 M. S. Anderson, *Appl. Phys. Lett.*, 2000, **76**, 3130–3132.
6 A. Weber-Bargioni, A. Schwartzberg, M. Cornaglia, A. Ismach, J. J. Urban, Y. J. Pang, R. Gordon, J. Bokor, M. B. Salmeron, D. F. Ogletree, P. Ashby, S. Cabrini and P. J. Schuck, *Nano Lett.*, 2011, **11**, 1201–1207.
7 M. Fleischer, A. Weber-Bargioni, M. V. P. Altoe, A. M. Schwartzberg, P. J. Schuck, S. Cabrini and D. P. Kern, *ACS Nano*, 2011, **5**, 2570–2579.
8 B. Ren, G. Picardi and B. Pettinger, *Rev. Sci. Instrum.*, 2004, **75**, 837–841.
9 L. T. Nieman, G. M. Krampert and R. E. Martinez, *Rev. Sci. Instrum.*, 2001, **72**, 1691–1699.
10 Y. M. You, N. A. Purnawirman, H. L. Hu, J. Kasim, H. P. Yang, C. L. Du, T. Yu and Z. X. Shen, *J. Raman Spectrosc.*, 2010, **41**, 1156–1162.
11 Y. Fujita, R. Chiba, G. Lu, N. N. Horimoto, S. Kajimoto, H. Fukumura and H. Uji-I, *Chem. Commun.*, 2014, **50**, 9839–9841.
12 R. M. Stockle, Y. D. Suh, V. Deckert and R. Zenobi, *Chem. Phys. Lett.*, 2000, **318**, 131–136.
13 B. S. Yeo, W. H. Zhang, C. Vannier and R. Zenobi, *Appl. Spectrosc.*, 2006, **60**, 1142–1147.
14 N. Hayazawa, M. Motohashi, Y. Saito, H. Ishitobi, A. Ono, T. Ichimura, P. Verma and S. Kawata, *J. Raman Spectrosc.*, 2007, **38**, 684–696.
15 M. Moretti, R. P. Zaccaria, E. Descrovi, G. Das, M. Leoncini, C. Liberale, F. De Angelis and E. Di Fabrizio, *Plasmonics*, 2013, **8**, 25–33.
16 W. H. Zhang, B. S. Yeo, T. Schmid and R. Zenobi, *J. Phys. Chem. C*, 2007, **111**, 1733–1738.
17 A. Hartschuh, H. Qian, C. Georgi, M. Bohmler and L. Novotny, *Anal. Bioanal. Chem.*, 2009, **394**, 1787–1795.

18 B. S. Yeo, S. Madler, T. Schmid, W. H. Zhang and R. Zenobi, *J. Phys. Chem. C*, 2008, **112**, 4867–4873.

19 B. Wiley, Y. Sun, B. Mayers and Y. Xia, *Chem. – Eur. J.*, 2005, **11**, 454–463.

20 Y. Fujita, P. Walke, S. De Feyter and H. Uji-i, *Jpn. J. Appl. Phys.*, 2016, **55**, 08NB03.

21 P. Walke, Y. Fujita, W. Peeters, S. Toyouchi, W. Frederickx, S. De Feyter and H. Uji-i, *Nanoscale*, 2018, **10**, 7556–7565.

22 A. W. Sanders, D. A. Routenberg, B. J. Wiley, Y. Xia, E. R. Dufresne and M. A. Reed, *Nano Lett.*, 2006, **6**, 1822–1826.

23 A. L. Pyayt, B. Wiley, Y. Xia, A. Chen and L. Dalton, *Nat. Nanotechnol.*, 2008, **3**, 660.

24 Y. Zhu, Q. Qin, F. Xu, F. Fan, Y. Ding, T. Zhang, B. J. Wiley and Z. L. Wang, *Phys. Rev. B: Condens. Matter Mater. Phys.*, 2012, **85**, 045443.

25 X. Z. Ma, Y. Z. Zhu, S. Kim, Q. S. Liu, P. Byrley, Y. Wei, J. Zhang, K. L. Jiang, S. S. Fan, R. X. Yan and M. Liu, *Nano Lett.*, 2016, **16**, 6896–6902.

26 Y. G. Sun, Y. D. Yin, B. T. Mayers, T. Herricks and Y. N. Xia, *Chem. Mater.*, 2002, **14**, 4736–4745.

27 K. E. Korte, S. E. Skrabalak and Y. N. Xia, *J. Mater. Chem.*, 2008, **18**, 437–441.

28 J. Wang, J. T. Jiu, T. Araki, M. Nogi, T. Sugahara, S. Nagao, H. Koga, P. He and K. Suganuma, *Nano-Micro Lett.*, 2015, **7**, 51–58.

29 S. M. Ansar, F. S. Arneer, W. F. Hu, S. L. Zou, C. U. Pittman and D. M. Zhang, *Nano Lett.*, 2013, **13**, 1226–1229.

30 M. H. Luo, Y. C. Hong, W. F. Yao, C. P. Huang, Q. J. Xu and Q. Wu, *J. Mater. Chem. A*, 2015, **3**, 2770–2775.

31 C. J. Chen, *Introduction to scanning tunneling microscopy*, Oxford University Press on Demand, 1993.

32 B. Wiley, T. Herricks, Y. G. Sun and Y. N. Xia, *Nano Lett.*, 2004, **4**, 2057–2057.

33 J. M. Gere and B. J. Goodno, *Mechanics of Materials*, Cengage Learning, USA, Brief edn, 2012.

34 S. Vlassov, B. Polyakov, L. M. Dorogin, M. Antsov, M. Mets, M. Umalas, R. Saar, R. Lohmus and I. Kink, *Mater. Chem. Phys.*, 2014, **143**, 1026–1031.

35 X. Z. Ma, Q. S. Liu, D. Xu, Y. Z. Zhu, S. G. Kim, Y. T. Cui, L. L. Zhong and M. Liu, *Nano Lett.*, 2017, **17**, 6961–6967.

36 J. Stadler, T. Schmid and R. Zenobi, *Nano Lett.*, 2010, **10**, 4514–4520.

37 P. B. Johnson and R.-W. Christy, *Phys. Rev. B: Solid State*, 1972, **6**, 4370.

Supporting Information

Ultra-sharp and surfactant-free silver nanowire for scanning tunneling microscopy and tip-enhanced Raman spectroscopy

Qiushi Liu*[1], Sanggon Kim*[2], Xuezhi Ma[1], Ning Yu[2], Yangzhi Zhu[2], Siyu Deng[1], Ruoxue Yan[2,3], Huijuan Zhao[4], Ming Liu[1,3]

Addresses:

[1]Department of Electrical and Computer Engineering, Bourns College of Engineering, University of California-Riverside, Riverside, California 92521, United States

[2]Department of Chemical and Environmental Engineering, Bourns College of Engineering, University of California-Riverside, Riverside, California 92521, United States

[3]Material Science Engineering program, Bourns College of Engineering, University of California-Riverside, Riverside, California 92521, United States

[4]Department of Mechanical Engineering, Clemson University, Clemson, SC 29634-0921, United States

*These authors contribute equally

Correspondence and requests for materials should be addressed to M.L. (email: mingliu@ucr.edu) and R.Y. (email:rxyan@engr.ucr.edu)

1. PVP removal from the AgNW tip region

Figure 2 shows the removal of PVP molecules from the AgNW sidewalls. Sidewalls were chosen to show the removal performance because it is known that PVP has higher binding energy with the sidewall {100} than the tip {111}[1, 2]. During the $NaBH_4$ bubbling treatment, the PVP at the AgNW tips are also efficiently removed. Figure S1a and b show the comparison of two AgNWs, without and with the $NaBH_4$ PVP-removal treatment, respectively.
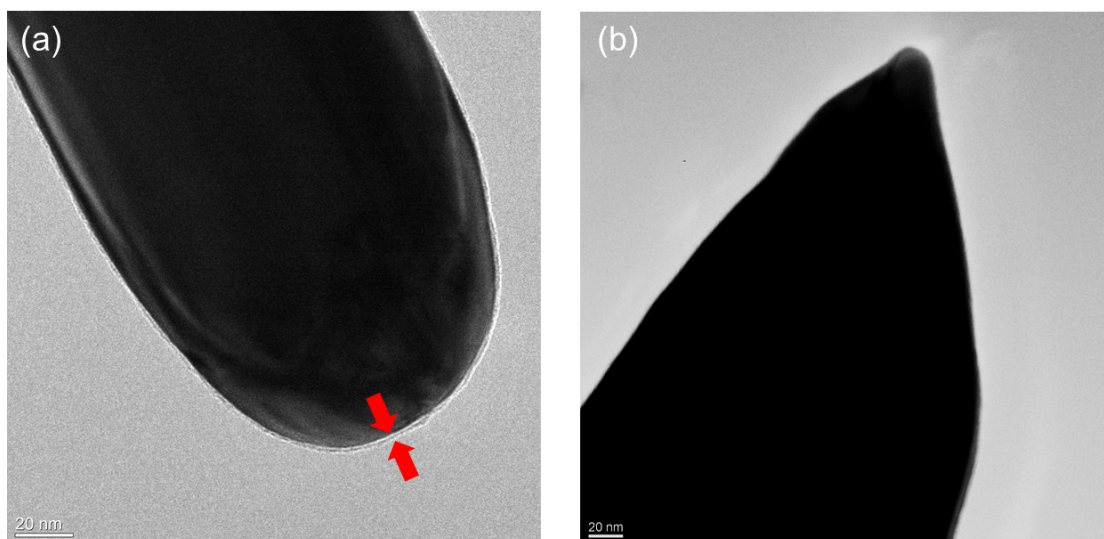

Figure S1. TEM images of the AgNW tips without (a) and with (b) the PVP removal treatment.

2. Influence of PVP to the STM performance

The influence of PVP layer on AgNW surface to the STM scanning results is shown in Figure 2. On the other hand, the PVP layer can also hinder the probe launching process, in particular with certain launching parameters, such as low bias voltage (<1V) and high tunneling-current setpoint (e.g. nA). Figure S2b shows the probe launching process with -0.5V probe voltage and 1nA target current, monitored by a high-magnification long-working-distance objective lens (Figure S2a). When the AgNW tip apex touches the Au substrate, the thin PVP layer reduces the tunneling current, resulting in the failure in triggering the abortion program to stop the probe approaching. As a result, the probe keeps approaching the substrate and bending the AgNW, until the Pt/Ir probe touches the substrate.

High bias voltage (Figure S2c, -1.5V) is sufficient for the probe launching process. However, even in this case, the long-chain PVP molecules at AgNW apex, despite multiple ethanol washing cycles, could not be removed by the high-voltage-pulse cleaning procedure, a cleaning method commonly used to remove molecules from STM probe tips, and the scanned images are similar in quality to Figure 2c-iii.
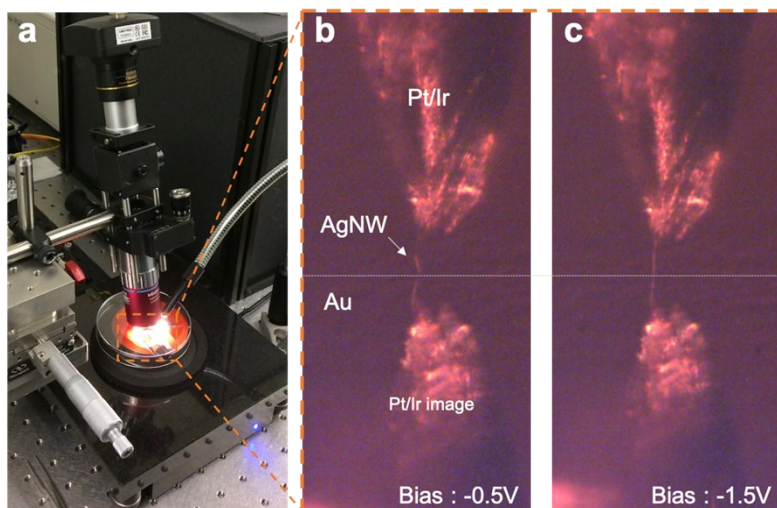
Figure S2 | The influence of PVP residues to the AgNW probe launching. a, The STM integrated with a long-working-distance objective lens for the monitor of the AgNW morphology during the STM probe launching. **b**, With low bias voltage (-0.5V on AgNW), the Pt/Ir probe kept moving towards the substrate, even after the AgNW tip apex touched the Au substrate, leading to a bent AgNW. **c**, With a higher bias voltage (-1.5V), the AgNW probe can be launched onto the Au substrate. However, the STM image quality is poor. The AgNW used here was pretreated 6 cycles of ethanol wash.

3. Influence from AgNW oxidation to the STM performance

The native oxide (Ag_2O) on silver exposed to the natural oxygen environment can quickly reach ~10 Å in thickness[3]. Ag_2O has a high electrical resistivity around 10^8 ohm·cm [4] and a bandgap around 1.5 eV [5], both of which prevent the tunneling current and restrict the STM performance. Therefore, although we do not observe any noticeable change in TEM (the TEM contrast of Ag and Ag_2O are very similar) between a freshly-prepared PVP-removed AgNW (Figure S3c) and a PVP-free AgNW that has been stored in air for 24 hrs (Figure S3d), we did see that the native oxide has a drastically influence the STM imaging quality. As displayed in Figure S3a, a fresh STM probe (within 10 mins of air exposure) could form clear image of the cluster morphology of the Au substrate. However, after exposed to the air for 2 hours, the oxidation layer on the AgNW surface impeded the tunneling current which results in the smeared STM image Figure S3b. Therefore, the AgNW-STM probe needs to be operated in inert gas environment or in vacuum, to prevent the oxidization.
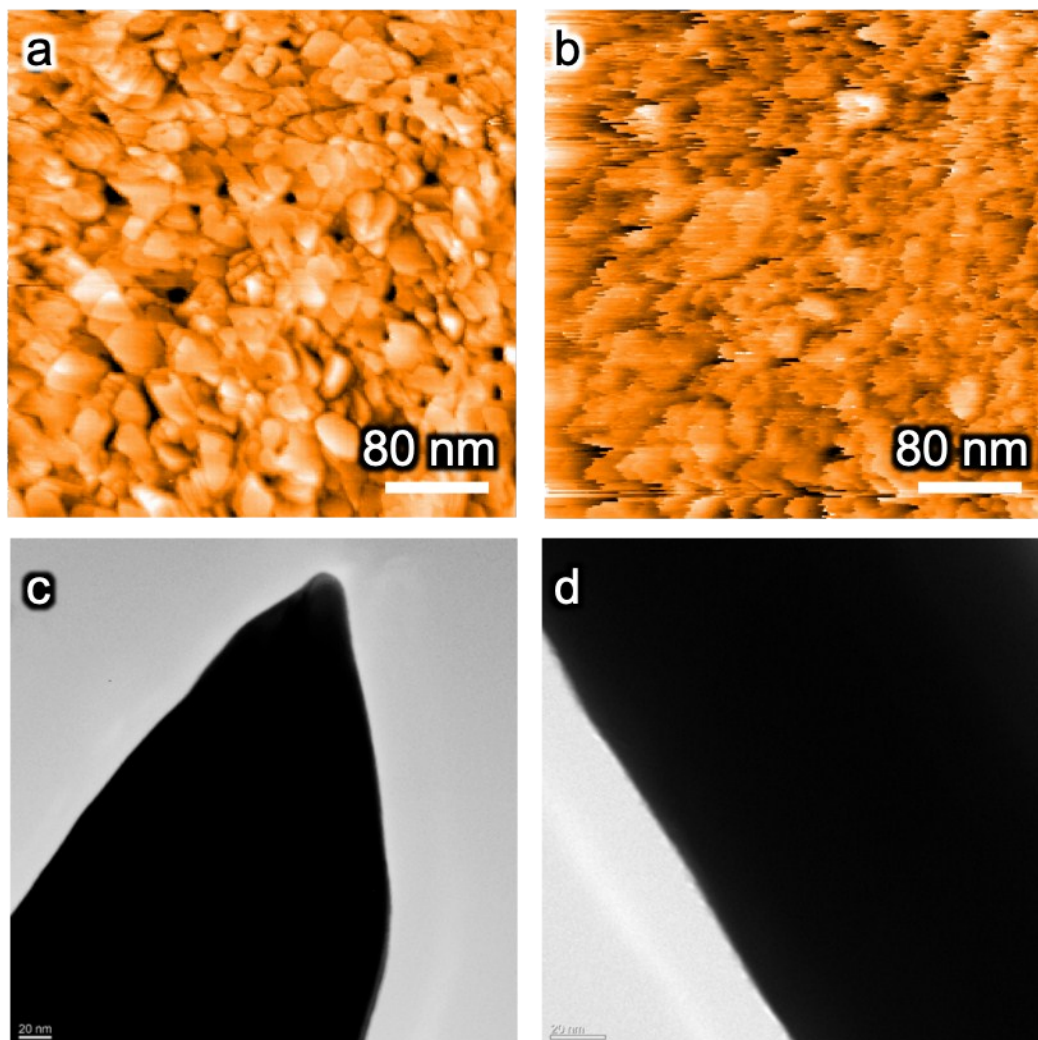
Figure S3 Oxidation of AgNW and its influence to STM imaging. **a**, STM image of a Au substrate, obtained by a freshly-prepared AgNW probe. **b**, The STM image acquired by the same probe after exposed to air for 2 hrs. **c**, TEM image of a freshly-cleaned AgNW. **d**, A PVP-removed AgNW, after stored in air for 24 hrs.

4. Influence of Tip radius to the STM performance

The regular AgNWs with large tip radii have a higher chance for the multiple-tunneling-channel effect, which not only smear spatial details, but also create ghost images. This effect can be seen in Figure S4a, which is an STM image of a gold surface scanned by a round-tip AgNW probe. The ghosting effect, as highlighted by the red rectangular, indicates that there are at least 3 tunneling channels that outline the same feature repeatedly. The estimated distance between channels is

around 10~20 nm, which is within the range of the tip radius of a flat tip, as shown in Figure S4b and c. The red arrows point to the possible locations of the multiple tunneling channels.
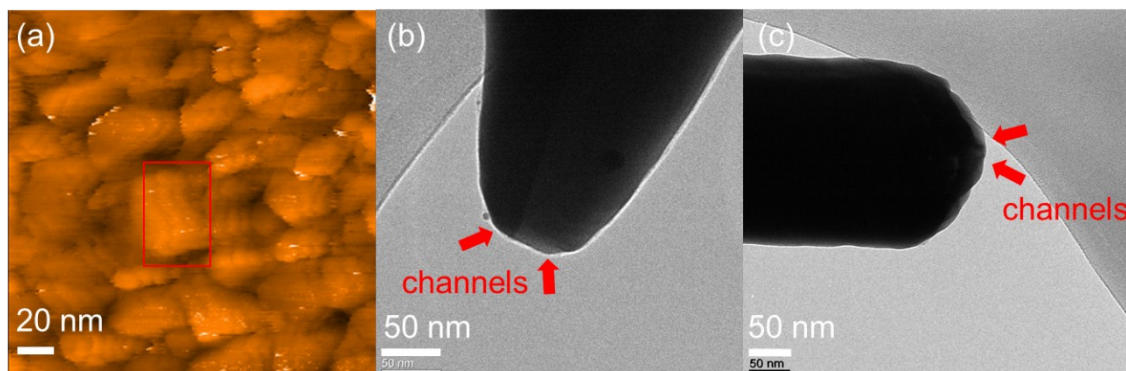

Figure S4. (a) STM result whose ghost comes from multi tunneling channels. (b) and (c) shows potential channels from round AgNW tip.

5. Repeatability of the TERS performance

In order to gain insights into the influence of the AgNW tip shape to the TERS experiment, five sharp-tip and five round-tip AgNWs have been tested. The measurements were conducted with contact-mode AFM (AgNW directly mounted on the cantilever). A monolayer graphene on 30 nm ultra-flat silver substrate was used as the evaluation sample. The TERS experiments were carried out using the same setup and parameters as described in the manuscript. A 532 nm green laser (~2 mW at the sample surface) is focused at the probe apex through a long-working-distance objective lens (NA=0.6). Both the sharp-tip and round-tip AgNWs were thoroughly cleaned through the $NaBH_4$ bubbling method, and the TERS experiments were conducted within 30 mins after the probe preparation to avoid oxidization.

The Raman signals from the graphene monolayer have been measured for each probe at ~5 different positions, with typical spectra shown in Figure S5a and c, for sharp-tip and round-tip probes, respectively. Figure S5b and d show the statistic of the 2D peak intensity measured with each probe for the sharp and the round tip AgNW probes respectively, with the standard errors indicated by the error bar and the original data listed in Table 1. Overall, the sharp-tip AgNW shows ~1480±140 counts, while the regular round tip probe shows 530±100 counts.
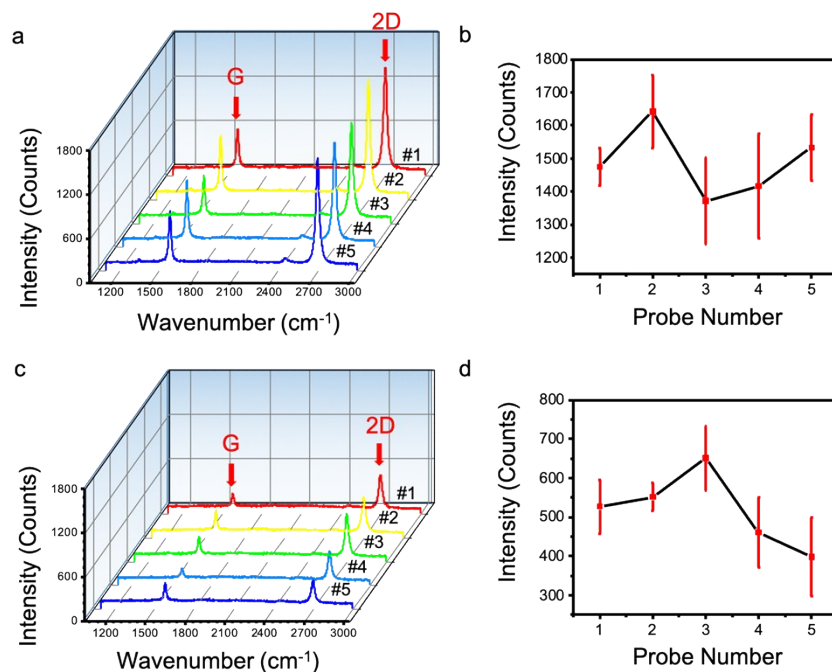
Figure S5. Monolayer Graphene Raman signal using (a) five sharp tip and (c) five round tip. (b) and (d) show each individual probe's 2D peak intensity distribution at different positions for sharp and round tips. Acquisition time = 3 sec

Table 1 Data from individual TERS probes (2D peak height in counts)

Location	Sharp#1	Sharp#2	Sharp#3	Sharp#4	Sharp#5	Rounded #1	Rounded #2	Rounded #3	Rounded #4	Rounded #5
1	1532.7	1774.9	1372.0	1306.0	1384.1	624.1	551.3	653.8	460.5	353.3
2	1520.8	1507.3	1622.2	1659.3	1532.6	526.7	625.1	692.7	421.0	398.1
3	1395.0	1642.0	1329.0	1416.3	1463.8	512.1	605.7	464.6	588.5	343.9
4	1424.1	1696.6	1328.7	1316.2	1592.7	542.0	587.5	651.1	563.1	560.1
5	1474.9	1542.0	1306.0	1264.1	1632.6	441.4	538.8	560.5	405.3	484.1
Stat.	1470 ± 60	1632 ± 110	1390 ± 130	1390 ± 160	1520 ± 100	530 ± 60	581 ± 36	600 ± 90	490 ± 80	430 ± 90

References:

1. Sun, Y., Gates, B., Mayers, B. & Xia, Y. Crystalline silver nanowires by soft solution processing. *Nano letters* **2**, 165-168 (2002).

2. Al-Saidi, W., Feng, H. & Fichthorn, K.A. Adsorption of polyvinylpyrrolidone on Ag surfaces: insight into a structure-directing agent. *Nano letters* **12**, 997-1001 (2012).

3. De Rooij, A. The oxidation of silver by atomic oxygen. *EsA Journal* **13**, 363-382 (1989).

4. Tvarusko, A. The electric resistivity of Ago. *Journal of the Electrochemical Society* **115**, 1105-1110 (1968).

5. Fortin, E. & Weichman, F. Photoconductivity in Ag2O. *physica status solidi (b)* **5**, 515-519 (1964).